Mechanics & Industry **26**, 38 (2025)
© L. Wang et al., Published by EDP Sciences 2025
https://doi.org/10.1051/meca/2025033

Mechanics & Industry

Available online at:
www.mechanics-industry.org

Original Article

Design and flow field characterization of safety valves based on the Laval principle

Lisong Wang[1], Zhuozhuo Qin[2], Hongguang Qi[2], Zengcheng Wang[2,*], Wenrui Jiang[2,*], Jiao Xu[3], Dameng Li[3], and Xin Jin[4]

[1] AVIC Harbin Dongan Engine Co., Ltd., Harbin, Heilongjiang 150066, PR China
[2] School of Mechatronics Engineering, Harbin Institute of Technology, Harbin, Heilongjiang 150001, PR China
[3] Harbin Power Valve Co., Ltd., Harbin Electric Corporation, Harbin, Heilongjiang 150090, PR China
[4] School of Mechanical and Power Engineering, Harbin University of Science and Technology, Harbin, Heilongjiang 150080, PR China

Received: 11 March 2025 / Accepted: 4 November 2025

Abstract. This paper designs a new type of safety valve suitable for ultra-supercritical conditions and analyzes its flow field characteristics through numerical simulation. The safety valve features a valve seat design based on the Laval principle, ensuring that the steam velocity at the outlet reaches supersonic speeds, thereby enhancing discharge efficiency. Using CFX software, in conjunction with a turbulence model and steady-state simulation techniques, an in-depth analysis of the fluid characteristics within the valve was conducted. The results show that under different pressure levels and valve openings, fluid characteristics such as pressure distribution and Mach number exhibit consistency. At the valve outlet, a distinct supersonic flow region was observed, verifying the superior pressure relief capacity of this safety valve design.

Keywords: Safety valve / supersonic / Laval nozzle principle / CFX simulation

1 Introduction

Safety valves serve as overpressure protection barriers for pressure-bearing equipment, with their performance being directly linked to the safe operation of the equipment and the effective prevention and control of accidents [1].

Beune A et al. [2] developed a numerical model of high-pressure safety valves to analyze their opening characteristics, revealing that significant forces can arise from the non-directional flow of large fluid volumes. Hoseinzadeh S et al. [3] proposed and designed an environmentally friendly fluid safety valve, using finite element analysis to investigate potential failure under maximum allowable working pressure. Gwon Hyeokrok [4] conducted numerical simulations of safety valves used in pressure regulating stations to analyze flow rate, lift, and the required effective discharge area, defining the maximum effective discharge area for safety valves. Song Yin et al. [5] utilized simulation methods to study the opening process of safety valves under high pressure. Hu Mingsen [6] proposed a high-precision safety valve testing architecture with three test channels and developed an automated testing system. Brenner Lorenz et al. [7] investigated passive air explosion safety valves. Choi Ji-Won et al. [8] employed conventional safety valves to predict discharge by establishing a balance equation between opening force and spring force, considering backpressure effects. Ma Haodong [9] used the FMEDA analysis method to examine the impact of various valve components on overall safety performance and proposed an optimization design method for improving safety valve reliability.

In recent years, CFD and multi-physics simulations have been widely applied in the analysis of complex flow systems. Pourmahmoud et al. [10] conducted numerical simulations of the Ranque–Hilsch vortex tube, revealing the influence of geometric parameters on temperature separation. Achour et al. [11] employed entropy production theory to analyze the energy loss and size effects of centrifugal pumps handling non-Newtonian emulsions. Dong et al. [12] established a multi-field coupling model to investigate the interactions among components, demonstrating their impact on pressure pulsation and vibration characteristics of the pump. In addition, recent studies on nonlinear dynamic systems, such as light-driven pendulum models based on liquid crystal elastomer fibers [13], provide insights into modeling energy-driven, self-excited motion in complex systems, offering methodological inspiration for analyzing transient and nonlinear responses in safety valves. These studies provide methodological references for

* e-mails: 23s108308@stu.hit.edu.cn; 3482235817@qq.com

This is an Open Access article distributed under the terms of the Creative Commons Attribution License (https://creativecommons.org/licenses/by/4.0), which permits unrestricted use, distribution, and reproduction in any medium, provided the original work is properly cited.

flow field simulation and performance optimization of safety valves operating under ultra-supercritical conditions.

Although current research has provided valuable insights and methodologies, studies on safety valves under ultra-supercritical conditions remain relatively scarce. This is a critical area that imposes higher demands on safety valve performance. Therefore, this paper focuses on the design and analysis of safety valves for ultra-supercritical units to gain a more comprehensive understanding of their performance characteristics and to provide practical guidance and support for engineering applications in related fields.

2 Design of ultra-supercritical safety valves

2.1 Structural improvements of safety valves

To meet the requirements of ultra-supercritical operating conditions, several structural modifications and optimizations were implemented, as illustrated in Figure 2.

- Valve Seat: Designed based on the Laval principle, as shown in Figure 1. This design enables the steam velocity at the outlet to reach supersonic levels.
- Valve Disc: A thermally-stressed compensation structure is employed, which produces minimal deformation when heated, improving the sealing condition of the valve disc and ensuring more stable and reliable performance in high-temperature environments.
- Upper and Lower Adjustment Rings: By adjusting the positions of both the upper and lower rings simultaneously, the valve's opening accuracy and reseating pressure can be precisely controlled under different operating conditions.
- Cooler: The cooler separates the spring from the valve body, preventing performance degradation or damage caused by temperature fluctuations, thereby maintaining the spring's stiffness and the overall stability of the valve's performance.
- Adjustment Sleeve: The position of the adjustment sleeve can be altered to change the resistance encountered by the valve disc during closing, ensuring precise reseating pressure when the valve closes.
- Valve Stem: The head of the valve stem is clad with hard alloy, enhancing the stem's impact resistance.
- Opening Mechanism: A manual opening handle is used to actively open the safety valve for purging operations.
- Locking Mechanism: A locking device is employed to secure the valve, preventing loosening during operation.

2.2 Displacement calculation of safety valves

To determine the valve opening size and calculate the flow rate of the safety valve, refer to relevant technical manuals such as the Safety Technical Supervision Regulations for Steam Boilers and the ASME Boiler and Pressure Vessel Code. These will help to derive the discharge pressure, reseating pressure, and other key parameters of the safety valve. The rated flow rate of the safety valve is calculated using steam as the medium. The required set pressure P_{set} is 35.5 MPa, which is greater than 11 MPa. The formula for calculating the discharge capacity of the safety valve is given by (1).

$$W = 0.5147 \times A \times (1.03 \times P_{set} \times 10.2 + 1) \times 0.9 \times C \times \alpha \tag{1}$$

In the formula, W represents the discharge capacity; A represents the discharge area; P_{set} represents the set pressure; C represents the steam correction factor; α represents the discharge coefficient. The formula for the discharge area of the safety valve is:

$$A = \frac{\pi d_t^2}{4} \tag{2}$$

The formula for calculating the discharge pressure is:

$$P_p = 1.03 \times P_{set} + 0.101 \tag{3}$$

In the formula, P_h represents the reseating pressure and ΔP_b represents the opening and closing pressure differential.

The discharge coefficient of the safety valve in (1) is related to various factors such as the valve structure, opening size, and the shape and dimensions of the flow passage. According to ASME standards, the maximum value of the discharge coefficient for a safety valve is 0.975. The steam correction factor C is taken as 0.794. Based on the design requirements, the set pressure $P_{set} = 35.5\ MPa$, and the throat diameter $A = 1809nm^2$. Using these parameters, the discharge area of the safety valve is calculated, and by substituting into (1), the discharge capacity is obtained as $W = 242579kg/h$, and the discharge pressure is calculated as $P_p = 36.67\ MPa$. The required opening and closing pressure differential should be between 4% and 7%. When the differential $\Delta P_b = 7\%$, the reseating pressure $P_h = 33.02MPa$; when the differential $\Delta P_b = 4\%$, the reseating pressure is calculated as $P_h = 34.08MPa$. This data supports the subsequent fluid simulation of the safety valve.

2.3 Emission reaction force calculation

When materials are released, the flow of liquid or gas generates a reaction force in the discharge pipeline, which is transmitted to the safety valve and forms a torque acting on the equipment nozzle.

$$F = \alpha_z \times \frac{A}{100} \times (1.03 \times P_{set} \times 10.2 + 1) - b, \tag{4}$$

In the equation: F represents the discharge reaction force; α_z represents the steam coefficient; A represents the discharge area; and b represents the flow area of the discharge pipe; D_o represents the diameter of the discharge pipe.

The calculation formula for the acting moment is:

$$M = FL, \tag{5}$$

In the equation: M represents the acting moment; L represents the distance from the center of the safety valve to the discharge pipe.

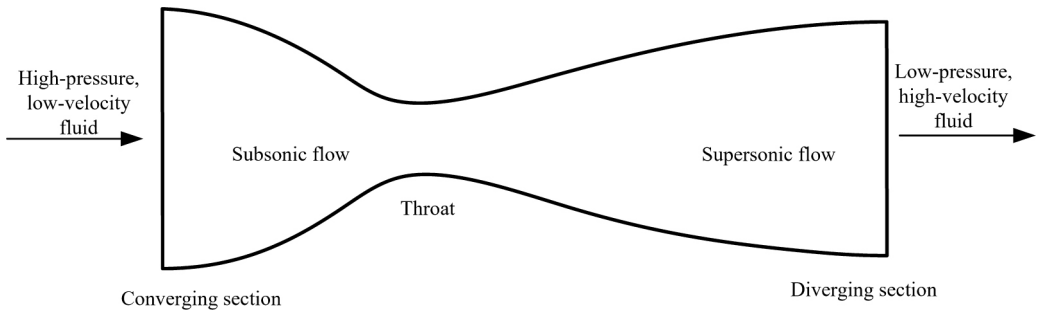

Fig. 1. Schematic diagram of the Rafael nozzle principle.

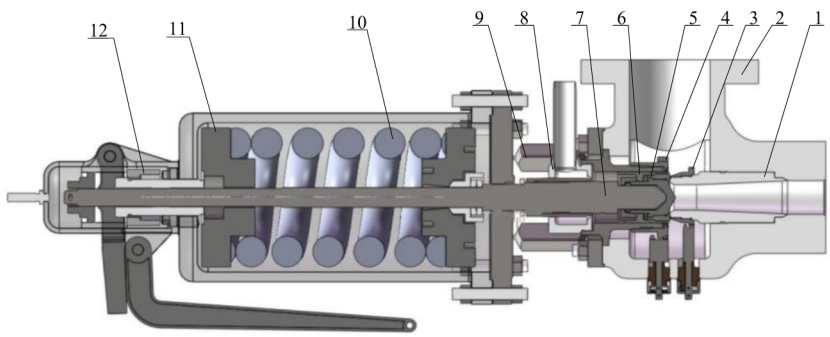

Fig. 2. Improved safety valve structure: 1 - Valve seat, 2 - Valve body, 3 - Lower adjustment ring, 4 - Upper adjustment ring, 5 - Valve disc, 6 - Adjustment sleeve, 7 - Valve stem, 8 - Exhaust chamber, 9 - Cooler, 10 - Spring, 11 - Spring seat, 12 - Locking device.

The distance from the center of the safety valve to the discharge pipe is:

$$L = C_s + 2 \times D_o \times 10 + 50. \tag{6}$$

In the equation: C_s represents the distance from the center of the safety valve to the outlet flange surface.

The diameter of the discharge pipe D_o is designed to be 15 cm, resulting in a flow area of the discharge pipe $b = 176.7cm^2$. Substituting this into the reaction force calculation formula (4), the discharge reaction force is calculated as $F = 8146.8kg$. The distance from the center of the safety valve to the outlet flange surface C_s is designed to be 254 mm, leading to a final reaction force moment of $M = 4920656kg{\cdot}mm$.

3 Establishment of a fluid simulation model

A numerical calculation model for a high-parameter spring-loaded direct-acting safety valve is established based on fluid mechanics methods and steady-state simulation techniques.

3.1 Establishment of the flow channel model

The 3D model in Figure 2 contains small gaps and complex structures due to design tolerances and assembly, which generally have minimal impact on fluid flow but may cause difficulties in mesh generation or overly dense local meshing. This increases analysis time and may even lead to failure. Therefore, the model must be simplified before extracting the computational domain. The simplified flow passage model is shown in Figure 3.

3.2 Simulation model selection

In this study, the Shear Stress Transport (SST) $k - \omega$ turbulence model is selected for the following fluid simulation analysis [14]. The main advantage of the SST model is that it accounts for turbulent shear stress, preventing excessive prediction of eddy viscosity [15,16]. Its transport behavior can be derived from the eddy viscosity equation containing a limiting number, as shown in (7):

$$v_t = \frac{a_1 k}{\max(a_1\omega, SF_2)}, \tag{7}$$

and

$$\nu_t = \mu_t/\rho. \tag{8}$$

In the equation: F_2 is a blending function, similar in function to F_1, and is used to constrain the limiting number in boundary layer regions for free shear flows where inappropriate assumptions may exist. S is an estimate of the strain rate.

The blending function F_1 is:

$$F_1 = \tanh(arg_1^4), \tag{9}$$

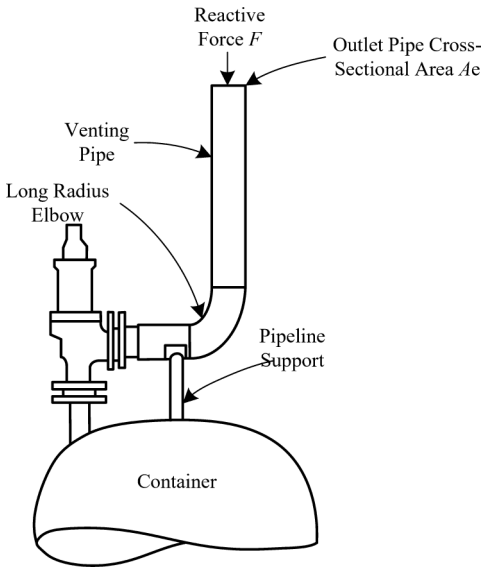

Fig. 3. Geometric modelling of internal runners.

and

$$arg_1 = min(\max(\frac{\sqrt{k}}{\beta\omega y}, \frac{500v}{y^2\omega}), \frac{4\rho k}{CD_{kw}\sigma_{w2}y^2}), \tag{10}$$

In the equation: y represents the distance to the nearest wall, and v denotes the kinematic viscosity.

$$CD_{kw} = \max(2\rho\frac{1}{\sigma_{\sigma_2}\omega}\nabla k\nabla\omega, 1.0 \times 10^{-10}), \tag{11}$$

$$F_2 = \tanh(arg_2^2), \tag{12}$$

$$arg_2 = \max(\frac{2\sqrt{k}}{\beta'\omega y}, \frac{500v}{y^2\omega}). \tag{13}$$

3.3 Mesh generation

Compared to structured grids, unstructured grids require less effort and offer better adaptability. Therefore, in this study, unstructured grids are used for discretization. In the global mesh settings, the overall mesh count is adjusted by changing the maximum and minimum mesh sizes, resulting in mesh counts of 0.12 million, 0.57 million, 1.16 million, 1.88 million, and 2.77 million. An example of the mesh distribution is shown in Figure 4.

A sparse mesh may lead to inaccurate capture of flow details and unstable numerical solutions, while excessive meshing in non-sensitive regions not only fails to improve accuracy but also significantly increases computational cost [17]. Therefore, taking the full open case as an example, a mesh independence study is conducted based on the five mesh models established above, with mass flow rate as the evaluation criterion, as shown in Figure 5.

As shown in Figure 5, the mass flow rate difference between 1.87 million and 2.76 million mesh elements becomes smaller. Through calculations, the mass flow rate difference between 1.16 million and 1.87 million mesh elements is 0.37%, while the difference between 1.80 million and 2.70 million mesh elements is only 0.13%. Therefore, it can be concluded that when the mesh count reaches 1.87 million or more, the impact of mesh count on the results can be considered negligible. Consequently, approximately 1.87 million mesh elements are used for flow field analysis in the subsequent flow channel models.

4 Analysis of flow field characteristics in the valve chamber under different pressures

According to the design requirements of the safety valve, with a set pressure of 35.5 MPa, the discharge pressure is calculated to be 36.67 MPa. At an opening and closing pressure differential of 4%, the reseating pressure is 34.08 MPa, and at a pressure differential of 7%, the reseating pressure is 33.02 MPa. This subsection will perform a steady-state simulation of the internal flow field of the safety valve based on these four pressure values. Three valve openings of 2 mm, 6 mm, and 11 mm will be examined to thoroughly demonstrate the variations in static pressure and velocity under different operating conditions of the safety valve, including when the valve disc is slightly opened, during the lifting or descending process, and when fully opened.

4.1 Static pressure analysis

The static pressure contour plot illustrates the pressure distribution within the flow field.

Figure 6 shows that as the inlet pressure decreases, the maximum static pressure of the safety valve at various openings gradually decreases. At small openings, the high-pressure gas at the inlet cannot flow sufficiently, and the minimum pressure remains balanced with the atmospheric pressure at the outlet pipe. As the opening increases to the critical value, the minimum static pressure also decreases with the reduction in inlet pressure. Overall, the pressure distribution in the flow field under different pressure conditions is relatively consistent.

At smaller openings, the pressure relief effect is insufficient, with the pressure differential concentrated below the valve disc. As the opening increases, fluid flow intensifies, and the pressure within the valve chamber gradually stabilizes. When the opening is at its maximum, the inlet flow passage exhibits a distinct pressure gradient, with pressure decreasing and stabilizing with the flow. This phenomenon can be explained by the variable cross-section flow characteristics in high-speed fluid dynamics. The maximum pressure is concentrated on the sealing surface of the valve disc. Figure 7 analyzes the maximum pressure under different pressure conditions.

Figure 7 illustrates the variation of maximum static pressure at different openings. Up to a valve opening of 4 mm, the maximum static pressure increases with the opening size. Between 4 mm and 6 mm, the pressure

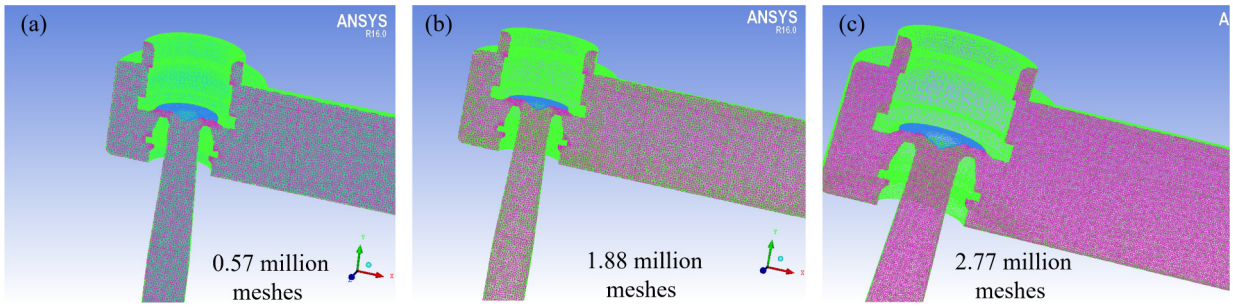

Fig. 4. Example of mesh division.

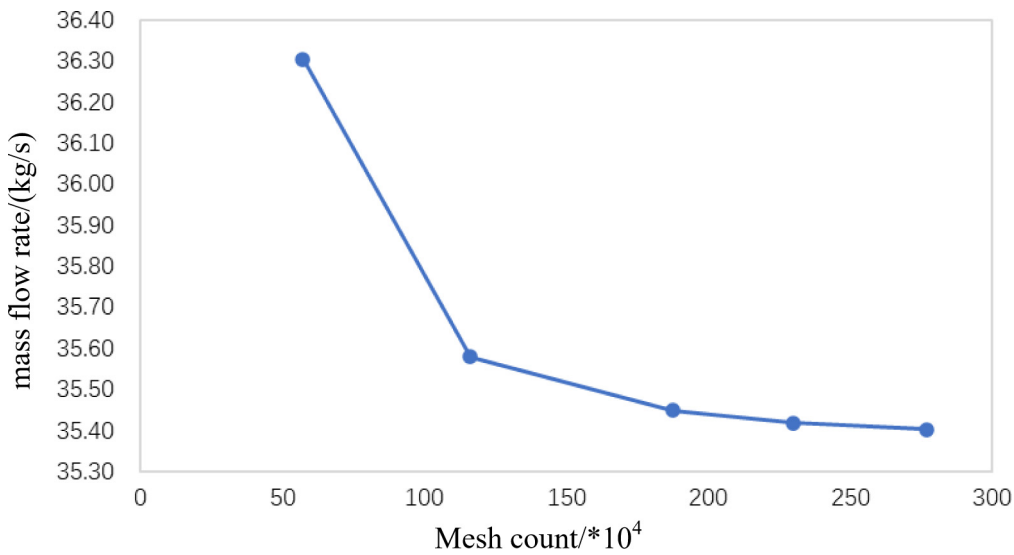

Fig. 5. Grid-independent analysis.

remains stable. When the opening exceeds 6 mm, the valve disc obstructs the flow, causing the maximum static pressure to increase again until the valve is fully open, at which point the system resistance disappears and the static pressure drops to the level of the inlet pressure. The trend of maximum static pressure variation at different pressures is similar.

4.2 Mach number analysis

The study of Mach number distribution provides further insights into the critical flow occurring within the safety valve.

Figure 8 shows that the variation of Mach number in the safety valve is similar under different pressures, with the maximum Mach number occurring at the outlet of the curtain passage, significantly influenced by the throttling effect. At small openings, the narrowing of the passage enhances the throttling effect, resulting in an increase in the maximum Mach number as the inlet pressure decreases. As the opening size increases, the throttling effect weakens, causing the maximum Mach number to decrease, although the sensitivity to pressure also diminishes. Regardless of the opening size, the maximum Mach number exceeds 1, indicating supersonic flow. In addition to the supersonic region at the curtain outlet, significant changes are also observed in the inlet flow passage, particularly at the throat. Taking the set pressure of 35.5 MPa as an example, five equidistant paths are established at the throat location of the safety valve, as shown in Figure 9, to analyze the variation of Mach number in different throat cross-sections under different openings.

As shown in Figures 10a and 10b, at opening sizes of 2 mm and 4 mm, there is no fluid flow in the paths L1 and L2 due to the proximity of the valve disc to the valve seat; therefore, it is unnecessary to extract Mach numbers for these paths. Overall, the variation trend of Mach numbers at the throat is consistent across different openings. Paths L1, L2, and L3 are located at the chamfer of the throat outlet, where the Mach number gradually increases from the center of the pipe toward the sides. Paths L4 and L5 are near the wall surface of the flow passage; due to the viscous effects of the wall, the Mach number decreases in the near-wall region, while it shows an increasing trend in the central section, resulting in a significant gradient change. The variation of the Mach number in path L1 is the most pronounced, becoming increasingly gradual as it moves further from the throat outlet. When the opening reaches

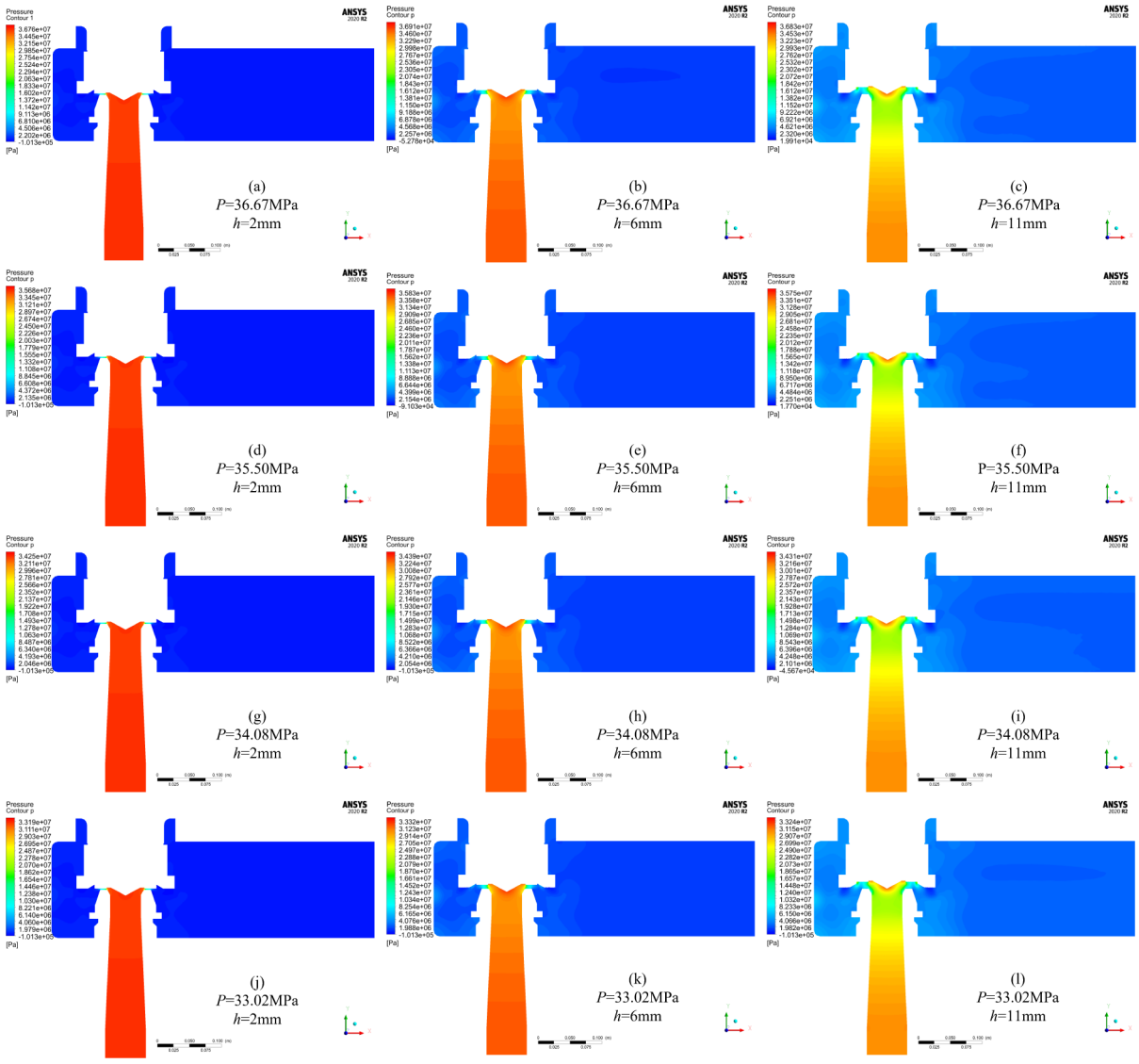

Fig. 6. Pressure cloud.

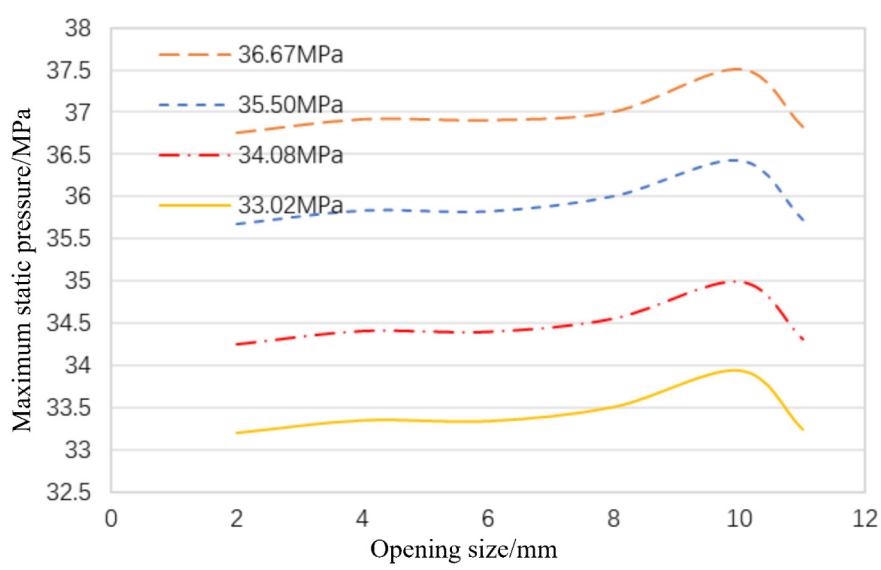

Fig. 7. Maximum pressure change curve.

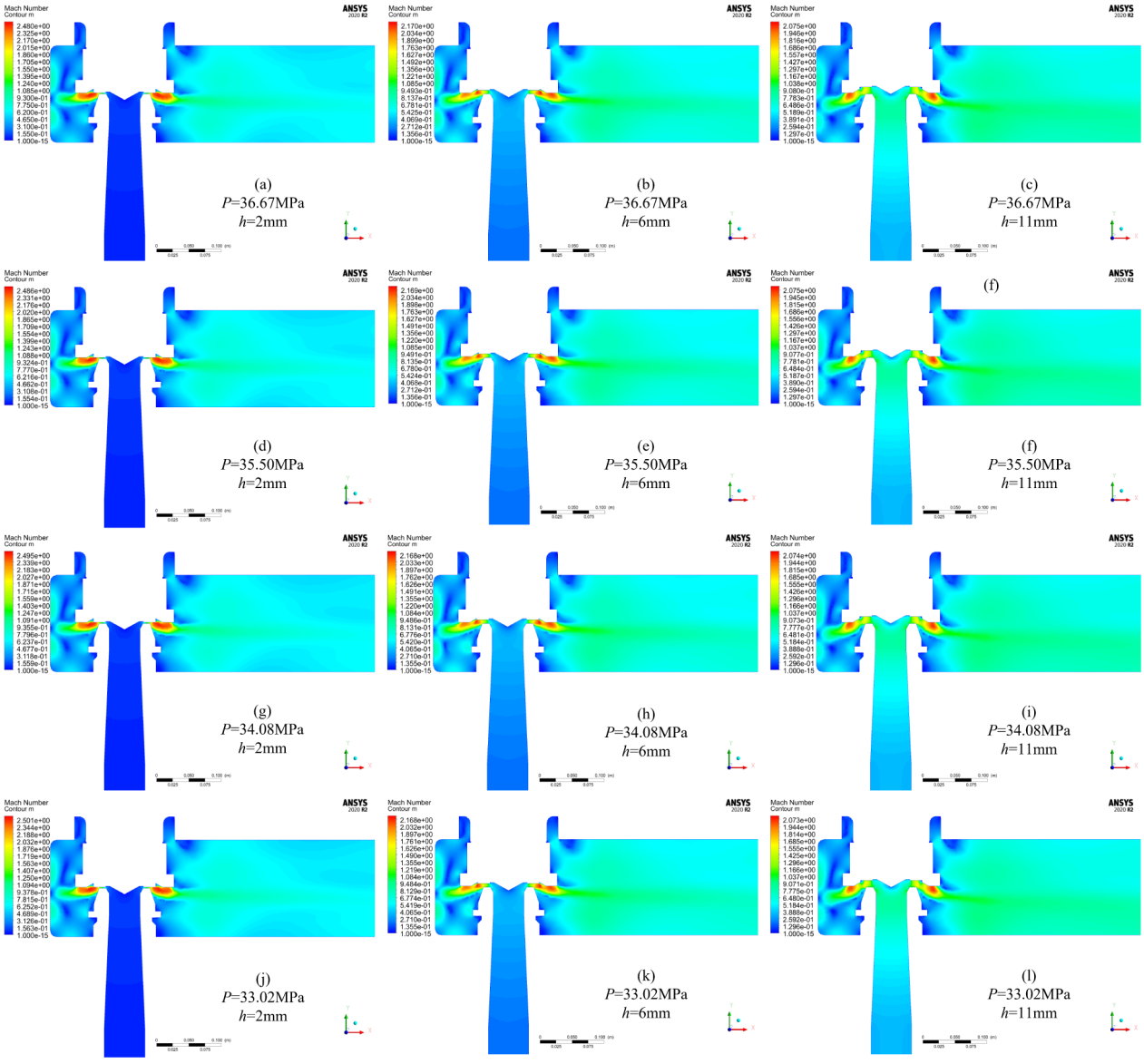

Fig. 8. Mach number cloud.

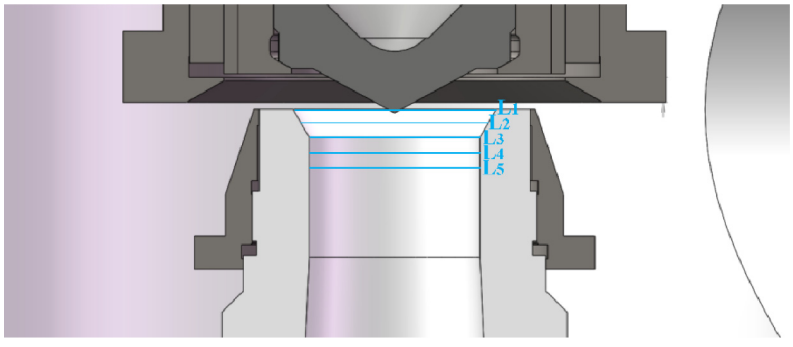

Fig. 9. Laryngeal path setting.

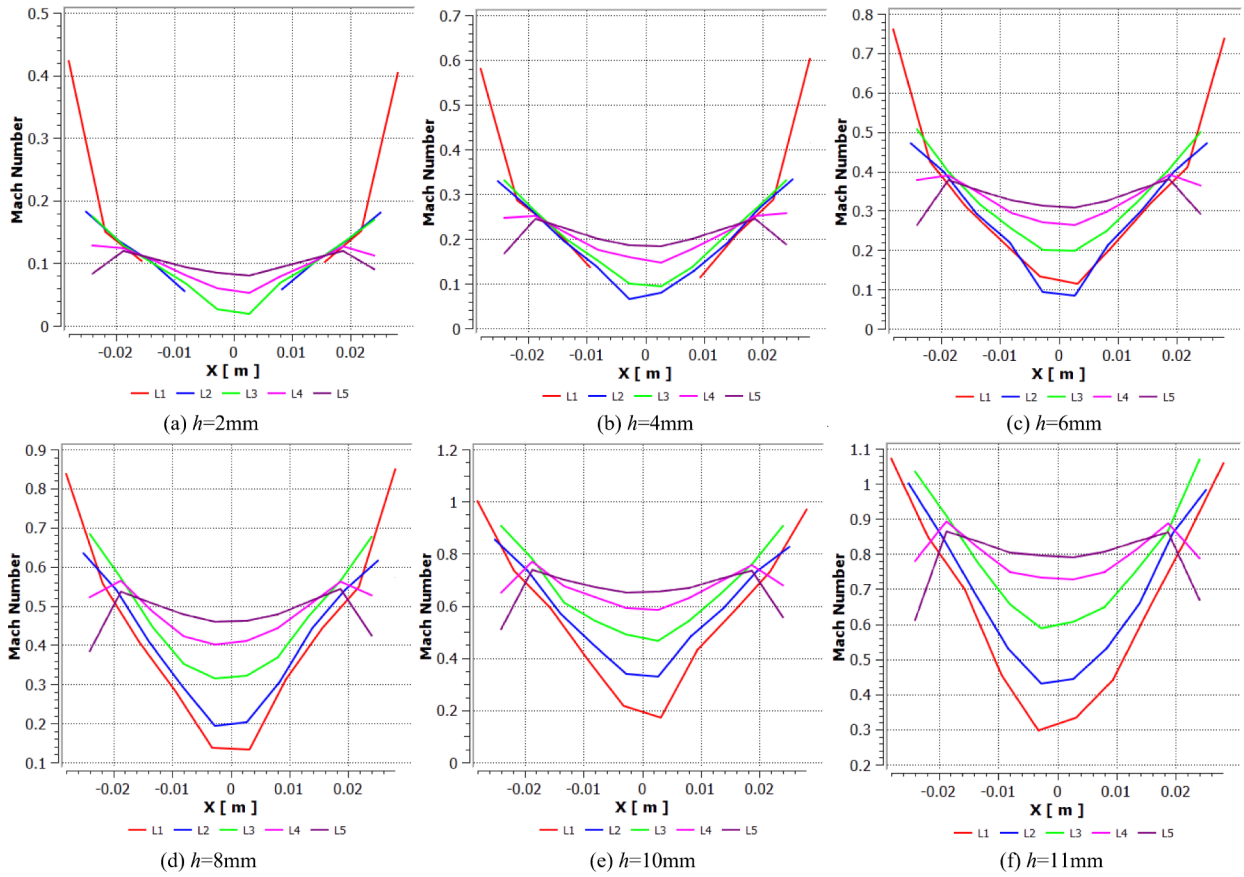

(a) h=2mm (b) h=4mm (c) h=6mm

(d) h=8mm (e) h=10mm (f) h=11mm

Fig. 10. Mach number variation curves over 5 paths in the larynx.

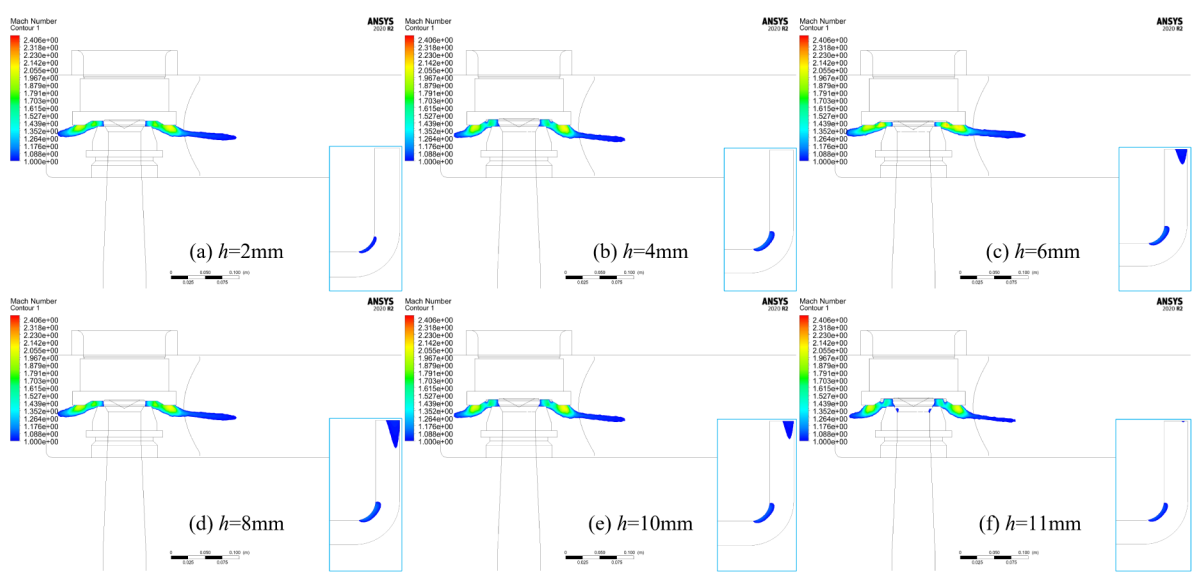

(a) h=2mm (b) h=4mm (c) h=6mm

(d) h=8mm (e) h=10mm (f) h=11mm

Fig. 11. Supersonic basin distribution.

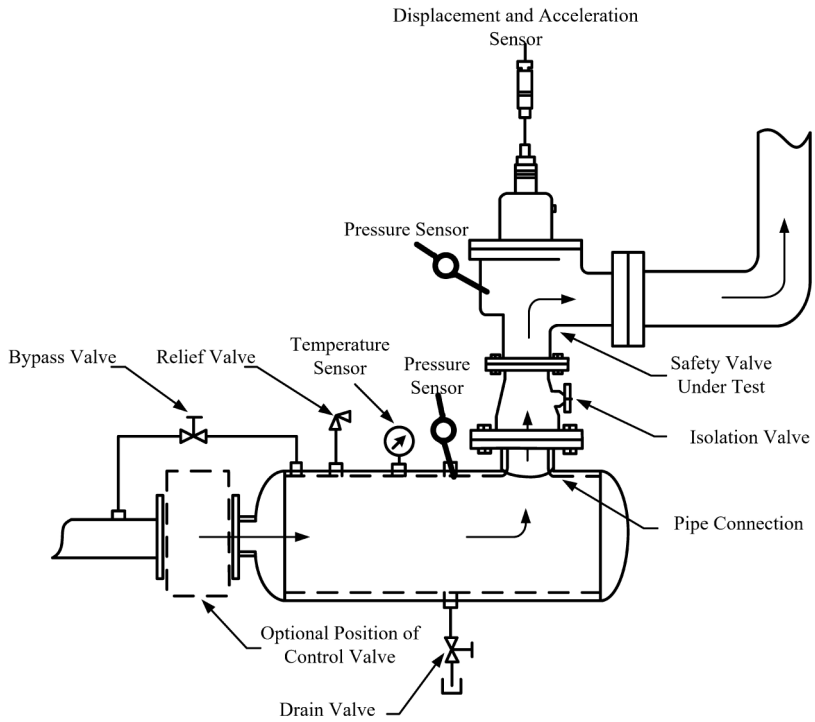

Fig. 12. Experimental setup diagram.

10 mm, the velocities at both ends of L1 approach the speed of sound. At full valve opening, the Mach numbers in parts of paths L1 and L2 exceed 1, indicating the presence of a supersonic region at the throat outlet. Figure 11 illustrates the distribution of the supersonic flow region where $Ma \geq 1$.

Figure 11 shows that the supersonic flow region is primarily located within the curtain passage and between the upper and lower adjustment rings of the valve body, gradually extending toward the outlet. In the lower right corner of each opening size, the supersonic region appears at the corner of the outlet pipe. As the opening increases, after the valve stroke reaches 6 mm, supersonic flow is also observed in the outlet pipe, indicating that the Laval principle seat enhances the steam discharge velocity and discharge coefficient, thereby improving the pressure relief capacity. At the throat, only a small supersonic region is present at the outlet chamfer under the fully open condition, while most of the throat remains in a subsonic state due to the significant flow resistance below the valve disc, resulting in higher pressure. In the outlet pipe, the medium accelerates after making a sharp turn, and as the discharge and opening size increase, the pressure decreases, satisfying the conditions for supersonic flow.

5 Experimental study

Experiments are a crucial step to validate the design and simulation results of the safety valve. The valve under study is intended for ultra-supercritical conditions, with a working medium temperature of 610 ℃ and a pressure of 35.5 MPa. However, currently available domestic high-temperature test facilities for safety valves can typically provide steam conditions of only about 10 MPa and 370 ℃, making it difficult to fully reproduce the actual operating conditions. Considering resource and safety constraints, this study conducts experiments under relatively lower parameter conditions, focusing on verifying the valve's pressure-relief capability and the reasonableness of the simulation model. Since direct comparison of flow velocity and temperature is challenging, the valve lift is selected as the primary metric for comparison.

5.1 Experimental setup

As shown in Figure 12, the experimental system consists of a DC boiler, a pressure vessel, control valves, a bypass valve, a drain valve, isolation valves, and the safety valve under test. The DC boiler provides superheated steam, which enters the pressure vessel after regulation by the control valve. When the pressure exceeds the design limit of the vessel, the pressure relief device is activated. The bypass valve can adjust both flow and pressure and facilitates maintenance of the safety valve during operation. The drain valve is used for rapid discharge of condensate and excess steam. The isolation valves are large-diameter gate valves without necking, which minimize additional pressure losses.

Pressure sensors are installed at the valve inlet to monitor the internal pressure in real time. Displacement and acceleration sensors are arranged at the top of the valve stem to capture the motion of the stem. All signals are

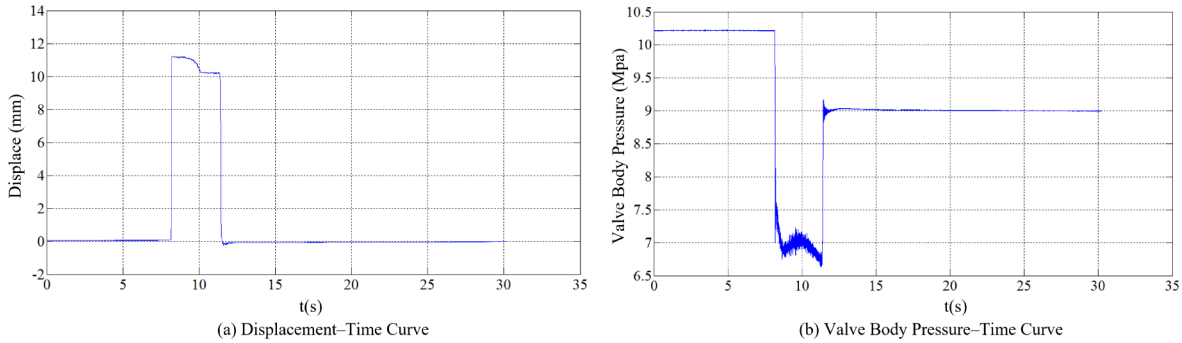

Fig. 13. Experimental result curves.

Table 1. Safety valve opening height and flap lift test data.

Opening height (mm)	Flap lift (N)	Opening height (mm)	Flap lift (N)	Opening height (mm)	Flap lift (N)
1	33423.8	5	35955.8	9	38031.3
2	36324.8	6	35529.7	10	39780.8
3	37198.4	7	35729.7	11	41376.7
4	36887.3	8	36658.4		

Table 2. Safety valve opening height and flap lift simulation data.

Opening height (mm)	Flap lift (N)	Opening height (mm)	Flap lift (N)	Opening height (mm)	Flap lift (N)
1	33678.1	5	37277.7	9	39954.4
2	36745.0	6	37122.1	10	41639.5
3	37477.9	7	37342.6	11	43080.1
4	37547.6	8	38470.4		

recorded and analyzed through a data processor, ensuring that the experiments are conducted safely within the specified pressure and temperature ranges.

5.2 Test data analysis

The displacement sensor recorded the opening and closing process of the safety valve, as shown in Figure 13. The results indicate that the valve lifted at 8.12 s, reaching a maximum opening height of 11 mm within approximately 22.3 ms, and reseated at 11.48 s. The pressure–time curve upstream of the valve shows a set pressure of 10.34 MPa and a reseating pressure of 9.17 MPa. The calculated opening–closing pressure difference is 11.3%, demonstrating that the valve responds quickly and operates stably.

Based on the measured displacement and acceleration data, the flap lift under different opening heights was calculated, and the average values of five tests are presented in Table 1. The corresponding lift data were further obtained by inputting the same conditions into the simulation model (Tab. 2). The comparison curve between experimental and simulated lift is shown in Figure 14. Experimental and simulated lift comparison curve.. The results indicate a consistent trend: the lift gradually increases at small openings, shows slight fluctuations in the 3–6 mm range, and then continues to rise. The simulation results are generally slightly higher than the experimental values, with the discrepancy increasing as the opening height increases.

The error analysis is shown in Figure 15, with the maximum relative error of 5.06%, which is within a reasonable range. The possible sources of error are as follows: (1) the friction coefficient in the simulation deviates from the actual value; (2) the back pressure effect on the valve disc is not fully considered; (3) the accuracy of the experimental equipment and environmental factors. Overall, the experimental results agree well with the simulation results, verifying the reliability of the established numerical model.

6 Conclusion

This study designs a novel safety valve suitable for ultra-supercritical conditions based on the Laval principle, and investigates its performance through numerical simulation and experimental validation. The main conclusions are as follows:

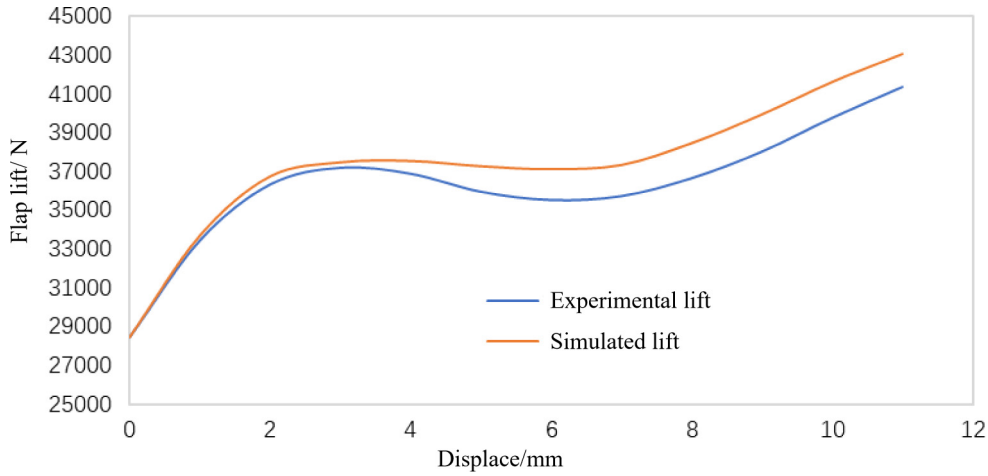

Fig. 14. Experimental and simulated lift comparison curve.

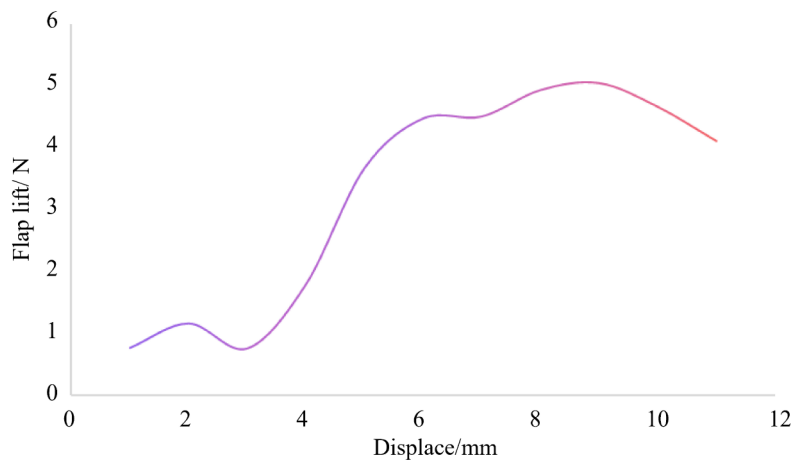

Fig. 15. Simulation error at different openings.

- Simulation results indicate that the flow field distribution of the safety valve is generally consistent under different pressures, with the maximum static pressure proportional to the inlet pressure and the maximum flow velocity inversely proportional.
- The valve opening has a significant influence on the flow field; as the opening increases, fluid flow is enhanced and the cavity pressure gradually stabilizes.
- Supersonic flow occurs in the curtain passage and at the valve outlet, verifying that the Laval-based seat design effectively increases steam discharge velocity and enhances the pressure relief capability.
- Experimental results are consistent with the simulation trend, with a maximum error of 5.06%, within a reasonable range, indicating that the established simulation model is highly accurate and can provide a reference for safety valve design and optimization. The flow field distribution of the safety valve remains relatively consistent under different pressure conditions, with the maximum static pressure being directly proportional to the inlet pressure and the maximum flow velocity being inversely proportional to it.

Funding

This research was funded by the Heilongjiang Provincial Key Research and Development Project (2022ZX01A13) and the Heilongjiang Provincial Natural Science Foundation Team Project (TD2023E002).

Conflicts of interest

No potential conflict of interest was reported by the authors.

Data availability statement

This article has no associated data generated and analyzed.

Author contribution statement

Conceptualization, L. Wang and Z. Qin; Methodology, Z. Qin and H. Qi; Software, Z. Wang and W. Jiang; Validation, W. Jiang, J. Xu, and D. Li; Formal Analysis, J. Xu and D. Li; Investigation, L. Wang and Z. Qin; Resources, X. Jin; Data Curation, Z. Wang and

W. Jiang; Writing – Original Draft Preparation, L. Wang and Z. Qin; Writing – Review & Editing, H. Qi and Z. Wang; Visualization, W. Jiang; Supervision, X. Jin; Project Administration, X. Jin.

References

[1] P.R. Sievert, The design of test equipment for safety and safety-relief valves, J. Press. Vessel Technol. 115, 147 (1993)

[2] A. Beune, J.G.M. Kuerten, M.P.C. van Heumen, CFD analysis with fluid–structure interaction of opening high-pressure safety valves, Comput. Fluids. 64, 108 (2012)

[3] S. Hoseinzadeh, S. Heyns, Developing a low-fluid pressure safety valve design through a numerical analysis approach, Int. J. Numer. Methods Heat Fluid Flow. 30, 1427 (2019)

[4] H.-R. Gwon, K.-C. Roh, Y.-S. Kim, S.-H. Lee, Numerical analysis for evaluation of ejection capacity relationship of safety valves in pressure regulating station (II) – Flow analysis and required effective discharge area of safety valve, J. Korean Inst. Gas. 12, 105 (2008)

[5] Y. Song, S.Y. Kwak, H. Hwang, A study on the optimization of safety valve structure through computational analysis, J. Comput. Fluids Eng. 26, 18 (2021)

[6] M. Hu, Design and development of a high-precision automatic safety valve testing system, Adv. Mech. Eng. 12, 1687814020914733 (2020)

[7] L. Brenner, C. Jenni, F. Guyer, P. Stähli, R. Eberlein, M. Huber, A. Zahnd, M. Schneider, F. Tillenkamp, Analysis of pressure drop and blast pressure leakage of passive air blast safety valves: an experimental and numerical study, J. Loss Prevent. Process Ind. 75, 104706 (2022)

[8] J.-W. Choi, S.-H. Jang, K.-H. Lee, Blowdown prediction of safety relief valve and FSI analysis, J. Korea Acad. Ind. Cooperat. Soc. 18, 729 (2017)

[9] H. Ma, Functional Safety Design Optimization and Internal Leakage Detection Research of Safety Valves, MS Thesis, China Academy of Launch Vehicle Technology, Beijing, China, 2020

[10] N. Pourmahmoud, A. Feyzi, A.A. Orang, A. Paykani, A parametric study on the performance of a Ranque-Hilsch vortex tube using a CFD-based approach, Mechanics & Industry 16, 203 (2015)

[11] L. Achour, M. Specklin, M. Asuaje, S. Kouidri, I. Belaidi, Energy loss analysis of volute centrifugal pump handling non-Newtonian emulsions through entropy production theory, Mechanics & Industry 25, 13 (2024)

[12] L.-Y. Dong, Z.-J. Shuai, T. Yu, J. Jian, Y.-B. Guo, W.-Y. Li, A multi-field coupling simulation model for the centrifugal pump system, Mechanics & Industry 24, 9 (2023)

[13] C. Bai, J. Kang, Y.Q. Wang, Light-induced motion of three-dimensional pendulum with liquid crystal elastomeric fiber, Int. J. Mech. Sci. 266, 108911 (2024)

[14] C. Zong, Dynamic Instability Analysis of Spring-Loaded Safety Valves Based on Fluid-Structure Interaction, PhD Thesis, Dalian University of Technology, Dalian, China, 2021

[15] C. Zong, F. Zheng, D. Chen, W. Dempster, X. Song, Computational fluid dynamics analysis of the flow force exerted on the disk of a direct-operated pressure safety valve in energy system, J. Press. Vessel Technol. 142, 011702 (2019)

[16] L. Xie, X. Zhao, ANSYS CFX Fluid Analysis and Simulation, Electronics Industry Press, Beijing, China, 2013

[17] K. Hu, Z. Li, ANSYS ICEM CFD Engineering Case Studies in Detail, Posts & Telecom Press, Beijing, China, 2014

Cite this article as: Lisong Wang, Zhuozhuo Qin, Hongguang Qi, Zengcheng Wang, Wenrui Jiang, Jiao Xu, Dameng Li, Xin Jin, Design and flow field characterization of safety valves based on the Laval principle, Mechanics & Industry **26**, 38 (2025), https://doi.org/10.1051/meca/2025033